Fabrication of P-Channel CMOS Perovskite Nanomaterials of $Sr_{0.5}$ $Mn_{0.5}$ Doped with PSB for High Efficient Energy Harvesting Photovoltaic Devices

Dr. Vinayak Adimule[1]*, Dr. Shwetarani R[2], Miss Anusha Suryavanshi [3], Mr. Adarsh HJ [4],

Abstract— In this research work a set of different compositional perovskite nanocomposite inorganic hybrid materials of Sr 0.5 Mn 0.5 (p-type) has been synthesized by co precipitation method using CTAB (cetyl trimethyl ammonium bromide) as surfactant, PSBs (pyridine Schiff base derivatives) 2-5% doped to the inorganic matrix. both the material was fabricated over titania dried ITO-Glass by RF spluttering and copper is deposited for the top contact and each of ITO-Glass is studied for the PCE parameters using solar simulator in dark and light illumination. Method: Inorganic Sr0.5 Mn0.5 nano compositional hybrid materials were prepared by co precipitation method, purified by washing with ethanol water mixture and the materials p-type and n-type were fabricated using spin coating and top contact is established by copper using RF sputtering. Initially characterized by cyclic voltammetry (CV), SEM and UV-Visible experiments. Studies related to power conversion efficiency (PCE) was measured with solar simulator to find the Pmax, Pmin, Vmax, I max, Jsc, and FF in dark as well as illuminated light source of frequency from 550 to 610 nm. Findings: Initial spectroscopic studies of CV showed the +ve oxidation potential for the p-type acceptor material and –ve oxidation potential showed for n-type material. UV-Visible studies showed the absorptive maxima for the doped perovskite nanomaterial is around 550-610 nm. FTO/TiO2/ Sr 0.5 Mn 0.5 /PSB is good photovoltaic performance under illumination with standard AM 1.5 sunlight. we obtained short circuit photocurrent densities as Jsc = 26.8 mA/cm2 and open circuit voltage Voc = 0.97 V , fill factor FF = 0.68 and a power conversion efficiency (PCE) of 10.60% under solar light intensity flux of 100 mW/cm2. The results of the present work suggest a route to realize a simple, low cost and highly efficient perovskite photovoltaic device. These devices could be realized in miniaturized sensors and electronic components applied in Internet of Things (IoT).

Index Terms— Nanocomposite, Flexible Device, Photovoltaic, Solar cell, Perovskite, IOT, Fabrication

1 INTRODUCTION

The energy has become an important in everyday life with increase in the population of world. The inevitable acceleration leads to its demand since, fossil fuel resources will eventually be depleted. Most of the energy used is currently derived from oil and coal [1]. Additionally coal combustion produces toxic nitrogen oxides and sulfur oxides as well as airborne particles [2]. Fossil fuels are also greenhouse gas emitters [3]. The greenhouse effect is the gradual heating of the earth due to increases in the concentration of a small portion of atmospheric gasses. These gasses, including water vapour, certain organic halides, and most crucially carbon dioxide [4-8], absorb reflected incident solar radiation that would otherwise pass back into space, and reemit the energy in the form of infrared radiation [8-12]. With the irresponsible or ignorant to take advantage of both materials, hybrid nanocomposites of inorganic semiconductors and conducting polymers are of great interest [13-15],

Especially as candidates for photovoltaic-cell materials, where the combined absorption band of both materials can also better harvest sun light. With this concept, conducting polymers have been combined with different inorganic semiconductors [16-18].

The current photonics based devices demand flexible optoelectronic components [19] that could be widely used in portable photovoltaics [20], display devices [21], flexible cell phones [22] and biosensors [23]. These materials are used for non-volatile switching memory device applications [24] and high-density data-storage devices. Thus, the energy harvesting ability of organic doped with inorganic materials with other device applications could prove a key enabler to the IoT, In addition, photo-induced charge separation mainly takes place at the interfaces between inorganic semiconductors and conjugating organic hybrid materials, where electrons are injected from the PSB organic into inorganic p-type semiconductors and holes remain in the PSBs. Actually, this interfacial charge separation can act some extent to prevent the recombination of separated electrons and holes.

.

2 MATERIALS AND METHODS

The material required for the synthesis are procured from Sigma Aldrich, spectrochem, SD-fine chemicals and used without purification. The FTO-Glass plates of 10-20ohm and dimension of 25 mm x 25 mm were procured from MG super lab Pune, the deposition of the top contact is done using RF spluttering instrument and semiconductor IVC measurements were carried out CENSE, IISc, Bangalore with the pellet size of 100 to 500 mm thickness. The solid supported SEM-EDX has

1*Dept. of Chemistry, JCET, Hubli-580031, Karnataka, India, E-mail: adimulevinayak@yahoo.in
2Scientist C, CNMS, , Bangalore-562112, Karnataka, India, E-mail: r.shwetha@jainuniversity.ac.in
2Dept. of Electronics and Communication, JCET, Hubli-580031, Karnataka, India
4NUI, Ireland (NUI), Ireland, H91TK33,

been done to closely understand the fusing of the material structures of p and n type of the materials. FTO glass substrates were cleaned in ethanol and deionized water and a sonicated. Anodes were fabricated on the FTO substrates by spin coating a drop of either nanoparticle in suspension as it is purchased, or semiconductor powder prepared as suspension. The spin coating was done at the rate 3000 rpm.

3 EXPERIMENTAL TECHNIQUES

3.1 Synthesis of Sr $_{0.5}$ Mn$_{0.5}$ doped with PSB

The equimolar concentrations Inorganic perovskite semiconductor Sr 0.5 Mn 0.5 was prepared by co precipitation method involving strontium carbonate and manganous sulphate reduced in presence of CTAB (cetyl trimethyl ammonium bromide) in reflux condition at 80-100° C as capping agent under acidic condition, precipitate was obtained which was washed thoroughly by water and the isolation is done by forming gelatinous network with NaOH and purifying it with ethanol water mixture. The pyridine Schiff base derivatives has been synthesized as described in figure 7 is made it in the form of hydrochloride and 2-5% of it is doped to the powdered nanocomposite material. The perovskite doped thin films were then deposited over FTO substrates by spin coating technique. The process is done repeatedly for the completeness of thin layer formation. About 120 µl solution was used to prepare the spin coated thin films at approximately 3000 rpm for 20 s, which were then annealed at 100°C for 15 min for each of the FTO plates. The perovskite films and powder of Sr 0.5 Mn0.5 and doped PSB were characterized by XRD, UV-visible spectroscopy, cyclic voltammetry and SEM measurements. Finally, the Sr 0.5 Mn0.5 doped with PSB was employed as an absorber in a 'hole-conductor free' photovoltaic device in miniaturation in IOT.

3.2 XRD analysis

Powder X-ray diffraction (XRD) measurement on the thin films was performed using Cu Kα radiation. The diffraction pattern for thin film Sr 0.5 Mn0.5 and doped with PSB is given in Fig.1. Most of the peak positions could be assigned to a tetragonal perovskite lattice structure using the crystal structure determination software powder-X.28 Using the Bragg-equation $n\lambda = 2d\sin\theta$ to find the inter-planar spacing d for peak positions (2θ) in the XRD data, lattice parameters were calculated by the formula 1d1d=h2+k2a2+l2c2h2+k2a2+l2c2 , and found to be $a = b = 9.661$ Å and $c = 13.564$ Å. The rest of the peaks could be attributed to the FTO substrate. A grain size of 35 nm was calculated using the Debye-Scherrer formula(τ=Kλβcosθ)(τ=Kλβcosθ) where K is a dimensionless factor close to unity, λ is the X-ray wavelength, β is the Full-Width at Half-Maximum and θ is the Bragg angle. Depending on the particle size, crystallinity. The semi-amorphous and the domain size can be significantly smaller. The diffraction pattern obtained above shows that Sr 0.5 Mn0.5 doped with PSB has good crystallinity.

3.3 SEM Spectral data of the Compounds

Scanning electron microscopy (SEM) studies of Sr 0.5 Mn0.5 perovskite nanomaterials were carried out by SEM measurement as shown in figure 2. SEM was performed using a Zeiss (Gemini 1550) microscope with a field emission electron source. The perovskite powder was obtained by drying a small amount (2 ml) from each of the two concentrations on a hot plate at 100°C. The average size of the crystallites was found to be ~50 nm, which matches the value obtained from XRD.

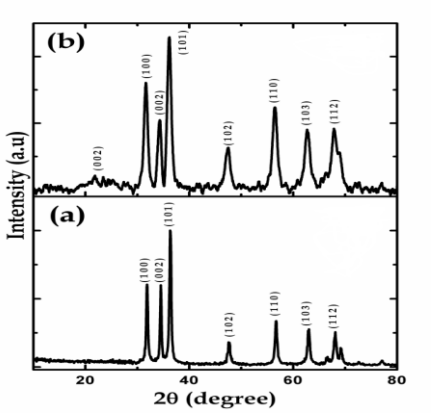

Fig.1. XRD patterns of the synthesized (a) Sr 0.5 Mn0.5 and (b) Sr 0.5 Mn0.5 doped with PSBs

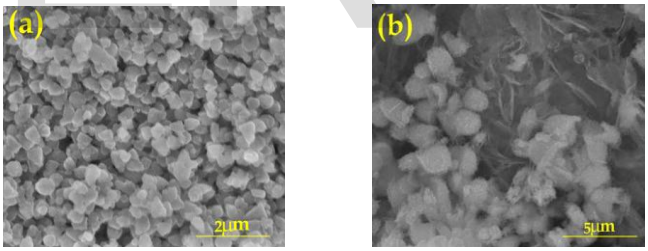

Fig. 2. SEM images of (a) Sr 0.5 Mn0.5 perovskite nanomaterials (b) Sr 0.5 Mn0.5 doped with PSB nanocomposite materials

3.4 Electrical characterization of fabricated photovoltaic device

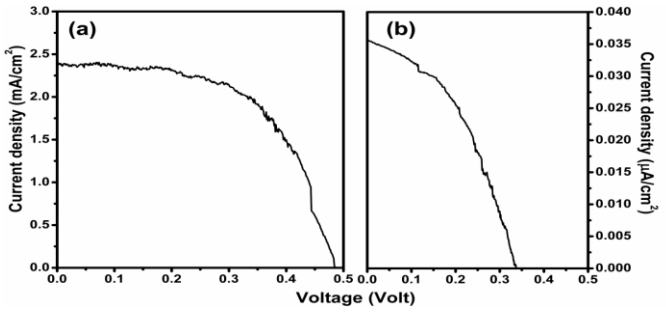

Fig. 3. J–V curves of the a) Sr 0.5 Mn 0.5 b) Sr 0.5 Mn 0.5 doped with PSB based on the different concentrations of PSB photoanodes.

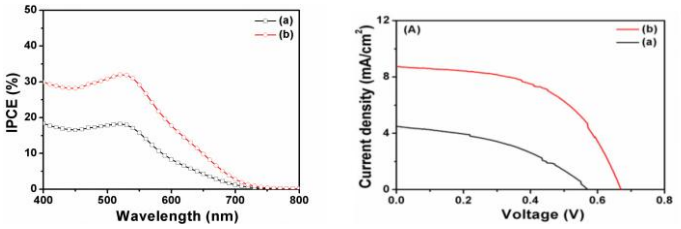

Fig. 4. J-V curve (a) Sr 0.5 Mn 0.5 doped with PSB based anodes (b) UV-visible wavelength of absorption Sr 0.5 Mn 0.5 doped with PSB based anodes

The current-voltage (I-V) characteristics of the perovskite devices were plotted in Fig. 4 .The I-V measurements were made using a Keithley source meter by applying an external potential bias to the cell and recording the generated photocurrent. The working and counter electrodes of the cell were connected to the source meter, and the cell mounted in the solar simulator. A 350 W Xenon lamp equipped with a sun filter (DC 350 Autosys) was used as a light source and a light intensity corresponding to one sun AM 1.0 (100 mW/cm2) was used to illuminate the cell surface.

4. APPLICATIONS OF PHOTOVOLTAIC CELLS

4.1 Gas Sensor Microchip Construction

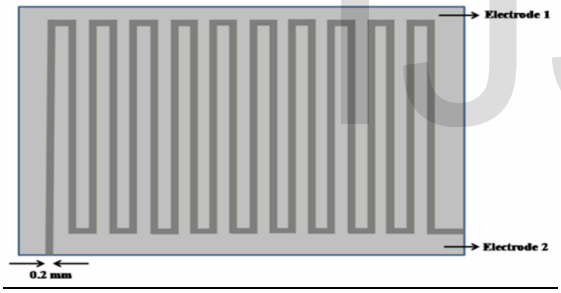

Fig. 5. Scheme of the constructed sensor microchip (gas sensing device).

A polyacrylamid plate (1 mm × 50 mm × 70 mm) was used as a base material of sensor device (microchip). Two copper comb electrodes were deposited on one side of the plate by the copper electroless process. The surface of copper electrodes was covered by gold electroplating. Figure 5 shows the scheme of gas sensing device.

We dispersed 0.2 g optimized Sr 0.5, Mn 0.5 doped with PSB nanocomposite in 5 ml acetone by ultrasonic shaking for 2 h to obtain a homogenous suspension (slurry). The surface of microchip was fully covered by the homogenized slurry. The microchip was kept in 100 °C for 10 min to evaporate the solvent to form a nanostructured thin film on the surface of the microchip. The coated microchip was cured at different temperatures (110, 120 and 130 °C) for 2 h to determine a suitable cohesion temperature of the Sr 0.5, Mn 0.5 doped with PSB nanocomposites, enabling them to adhere to one another and to the microchip surface.

The cured microchip was input into a glassy cubic box of 32 L total volume. A small electric fan was used to make fast homogenization of the gas mixture in the box. The different volumes of some gases, such as NH3, O2, H2O, CO, H2, and LPG were injected into the box, and the sensor resistance was measured.

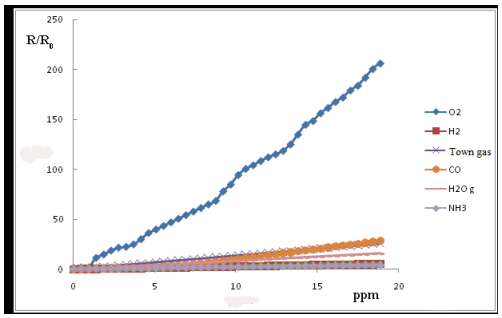

Fig. 6. The sensor response for different concentrations of various gases at temperature of 128 ºC.

The effect of variations in O2 concentration was investigated on the sensor resistance at 25, 65, and 130 °C and the linear range of the obtained results were represented in Fig. 6. It is obvious in Fig. 6, by increasing the measuring temperature, the sensor ability is increased.

For more clarifications, the linear ranges of the sensor response versus oxygen concentration were shown in Fig. 6. As we see in this figure, by increasing the measuring temperature, the linear range and the response sensitivity (the slope of calibration curve) are improved. It should be mentioned, at higher temperature the substrate of microchip shrink. At temperature of 130 °C, the curve shows a maximum slope and consequently, the most sensitivity to oxygen.

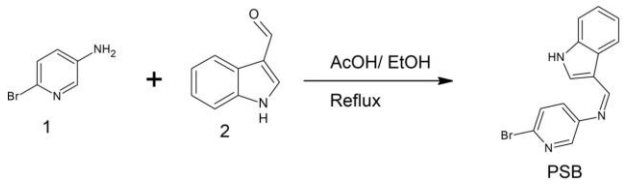

Fig. 7. Synthetic Pathway of the Pyridine Schiff base derivatives

Table 1. Results of sensor application for measurement of O_2 in presence of CO, N_2 and LPG

Experiment No	Initial Concentration of oxygen (ppm)	Resulted Concentartion of oxygen (ppm)
1	8	8.04
2	8	8.07
3	8	8.12

4. RESULTS AND DISCUSSIONS

In this work we have synthesized the hybrid organic-inorganic perovskite semiconductor material and studied it by structural, optical and morphological characterization techniques. Figure 3 and 4 shows the J-V curves of the interconnected grid-type perovskite modules and the corresponding J-V parameters are summarized in Table 1. For comparison, the individual J-V curve of is also measured by masking either the left or the right part of the module, using a piece of black plastic. From Table 1, it is seen that the open circuit voltage (VOC) of the entire module is 2.17 V, the short circuit current (ISC) is almost 320 mA, the fill factor (FF) is 0.68 and the power conversion efficiency (PCE) reaches 10.60 which indicates that the fabrication process is stable and reproducible. Perovskite materials and techniques involved are not limited to perovskite solar cells only, but these meet the requirements of potential electronic materials and their fabrication which will produce elastic, fracture-proof, light weight and environment friendly power sources in indoor customer electronics, flexible photovoltaics, bio-sensors and bio-medical devices.

TABLE 1

Table 1: The photocurrent density (Jsc), open-circuit voltage (Voc), fill factor (FF) and efficiency of pervoskite and doped pervoskite working electrodes

Sample	J_{sc} (mA/cm2)	V_{OC} (V)	FF (%)	η (%)
$Sr_{0.5}Mn_{0.5}$	10.4	0.38	0.29	2.35
$Sr_{0.5}Mn_{0.5}$ 2% PSB	18.4	0.55	0.34	4.69
$Sr_{0.5}Mn_{0.5}$ 3% PSB	20.6	0.66	0.49	7.60
$Sr_{0.5}Mn_{0.5}$ 4% PSB	22.8	0.87	0.50	8.10
$Sr_{0.5}Mn_{0.5}$ 5% PSB	26.6	0.97	0.68	10.60

5. CONCLUSION

A new series has been developed with hybrid organic-inorganic perovskite semiconductor p-n composite material of good performance. Solar cell performance tests indicate that Sr 0.5 Mn0.5 5% PSB the sensitized solar cell is better than the DSSC sensitized solar cell with highest PCE of 10.60%. Good photoelectric performance. (i) Increase in contact area between mesoporous TiO2 and FTO substrate via the perovskite layer, (ii) effective hole-blocking perovskite by the TiO2 layer, (iii) the presence of effectively continuous electron pathways within the TiO2 layer, and (iv) reduced leakage of carriers by the perovskite which prevents direct contact between the Sr 0.5 Mn0.5 PSB absorber and the conducting substrate. This study establishes the significance of the introduction of the compact layer in improving device efficiency.

6. ACKNOWLEDGEMENTS

This research work was supported by Defence Research Development Organisation. The Cyclic voltammetry Experiments were performed in KLE Institute of Technology, Hubballi, SEM, Semiconductor IVC and related electronic experiments were carried out at centre for nano science and engineering (CENSE), IISc, Bangalore, Karnataka, India. All the co-authors are thankful to all the mentioned supporting organizations for carrying out this research work.

7. CONFLICT OF INTEREST

All authors declare that they do not have any conflict of interest

REFERENCES

1. A.E. Shalan, "A facile low temperature synthesis of TiO2 nanorods for high efficiency dye sensitized solar cells." Applied Physics A. pp. 111-122, 2013.
2. M. Wright, A. Uddin, "Organic-inorganic hybrid solar cells: A comparative review". Solar Energy Matter. Solar Cells, pp. 87–111, 2012.
3. C. Deibel, T. Strobel, V. Dyakonov, "Role of the charge transfer state in organic donor-acceptor solar cells", Advanced. Materials. pp. 4097–4111, 2010.
4. R.K. Bhardwaj, H.S. Kushwaha, , J. T. GaurUpreti, , V. Bharti, V. Gupta, N. Chaudhary,.; G.D Sharma, K.Banerjee, S. Chand, "A green approach for direct growth of CdS nanoparticles network in poly (3-hexylthiophene-2,5-diyl) polymer film for hybrid photovoltaic". Material Letters., pp. 195–197, 2012.
5. X. Cao, N. Wang, X. Kim, "Mesoporous CdS spheres for high-performance hybrid solar cells". Electrochimica. Acta, pp. 9504–9507, 2011.
6. F. Chen, W.M Qiu, X.Q. Chen, L. G.Yang, X.X. Jiang, M. Wang, H. Z. Chen, "Large-scale fabrication of CdS nanorod arrays on transparent conductive substrates from aqueous solutions". Solar Energy, pp. 2122–2129, 2011.
7. G.D. Sharma , P. Suresh , S. K. Sharma, M.S. Roy, " Photovoltaic properties of liquid-state photo electrochemical cells based on PPAT and a composite film ofPPAT and nanocrystalline titanium dioxide", Synthetic Metals, pp. 509–515, 2008.
8. M. Trznadel, M. Zagórska, M. Lapkowski, G. Louarn S. Lefrant A. Pron, "UV–VIS–NIR and Raman spectro electrochemistry of regioregular poly (3-octylthiophene): Comparison with its non-regioregular analogue". Journal of the Chemical Society, Faraday Transactions, pp. 1387–1393, 1996. DOI: 10.1039/FT9969201387
9. G. Choudalakis, A. D. Gotsis, "Permeability of polymer/clay nanocomposites: A review", European Polymer Journal, pp. 967- 84, 2009.
10. R. Sothornvit R, S. I. Hong SI, D. J. An J. W. Rhim. "Effect of clay content on the physical and antimicrobial properties of whey protein isolate/organo-clay composite films" . LWT Food Science and Technology. pp. 279-84, 2010.
11. S.S. Aliabadi, M. A. Mohammadifar, H. Hosseini, A. Mohammadi , G, Mehran , S. M. Hosseinia, H, Mehrdad, K. Ramin K. "Characterization of nanobiocomposite kappa-carrageenan film with Zataria multiflora essential oil and nanoclay" .International Journal of Biological Macromolecules. pp. 282-89, 2014.
12. L. Sang-Rock, P. Hwan-Man, L. Hyuntaek, K, Taekyu, L. Xiucuo, C. Won-Jei, C. S. Ha "Microstructure, tensile properties, and biodegradability of aliphatic polyester/clay nanocomposites" . Polymer. pp. 2495-500, 2002.
13. M. Atef, M. Rezaei, R. Behrooz. "Characterization of physical, mechanical, and antibacterial properties of agar-cellulose bio nanocomposite films incorporated with savory essential oil" . Food Hydrocolloids.:pp. 150-57, 2015
14. A. Heydari,, I. Alemzadeh, M. Vossoughi, " Functional properties of biodegradable corn starch nanocomposites for food packaging applications" . Materials and Design, pp. 954-961, 2015.

15. J.W. Rhim, S.I. Hong, C.S. Ha. "Tensile, water vapour barrier and antimicrobial properties of PLA/nanoclay composite films". LWT - Food Science and Technology. pp.612-17, 2011.
16. A. L. Incoronato, A. Conte, G.G. Buonocore, M. A. Del Nobile. "Agar Hydrogel with Silver Nanoparticles to Prolong the Shelf Life of Fior Di Latte Cheese. Journal of Dairy Science, pp. 1697-1704, 2011.
17. J. Jayaramudu, G.S. M. Reddy, K, Varaprasad, E.R. Sadiku, S.S. Ray, A. V. Rajulu, "Preparation and Properties of Biodegradable Films from Sterculia Urens Short Fiber/Cellulose Green Composites". Carbohydrate Polymers pp. 622-627, 2013.
18. M. Jorda-Beneyto, N. Ortuño, A. Devis, S. Aucejo, M. Puerto, D. Gutiérrez-Praena, J. Houtman, S. Pichardo, S. Maisanaba, A. Jos, "Use of Nanoclay Platelets in Food Packaging Materials: Technical and Cytotoxicity Approach. Food Additives and Contaminants" - Part A Chemistry, Analysis, Control, Exposure and Risk Assessment pp. 354-363 2014.
19. J.Y. Kim, K. Lee, N.E. Coates, D. Moses , T.Q. Nguyen , M. Dante A.J. Heeger "Efficient tandem polymer solar cells fabricated by all-solution processing. Science", pp. 222–225, 2007. DOI: 10.1126/science.1141711
20. S.W. Hwang, Y. Chen, "Synthesis and electrochemical and optical properties of novel poly(aryl ether)s with isolated carbazole and p-quaterphenyl chromophores. Macromolecules, pp. 2981–2986, 2001. DOI: 10.1021/ma001855z
21. C. J. Shi, Y. Yao Y, Yang, Q. B. Pei , "Regioregular copolymers of 3-alkoxythiophene and their photovoltaic application" . Journal of the American Chemical Society, pp. 8980–8986, 2006. DOI: 10.1021/ja061664x
22. R. Mehdi, H. Youssef, M. B. Naceur, E. Ghanbar, A. N. Karimi, D. Alain, . "Cellulose whiskers reinforced polyvinyl alcohol copolymers nanocomposites". European Polymer Journal. pp. 2489-98,2008.
23. G. Kfoury, J.M. Raquez, F. Hassouna, J. Odent, V. Toniazzo, D. Ruch, P. Dubois, "Recent Advances in High Performance Poly(lactide): From "Green" Plasticization to Super-Tough Materials via (Reactive) Compounding". Frontiers in Chemistry, pp. 1-46. 2014.
24. W. Ya-Nan, W. Yun-Xuan, W. Lei, "Characterization of interfacial compatibility of polylactic acid and bamboo flour (PLA/BF) in bio-composites". Polymer Testing. 119-25, 2014.